J. Meas. Sci. Instrum., 2025, 16(1): 75-84. http://jmsi.publish.founderss.cn/
DOI: 10.62756/jmsi.1674-8042.2025008 jmsi@nuc.edu.cn

Double-channel cyclic image deblurring algorithm based on edge features

LI Jiamin, HU Hongping*, BAI Yanping
School of Mathematics, North University of China, Taiyuan 030051, China

***Corresponding author:** HU Hongping (hhp92@163.com)

Received: June 5, 2024 **Revised:** August 14, 2024 **Accepted:** September 4, 2024

Abstract: Photographs taken in daily life often became blurred due to shaking, out-of-focus, changes in depth of field, and movement of photographed objects. Aiming at this problem, a double-channel cyclic image deblurring method based on edge features was proposed. Firstly, image edge gradient operator was introduced as a threshold based on the rule that the maximum value of the image edge gradient will decrease after the blurring process, making the blurred image be divided into two channels: edge channel and non-edge channel. Secondly, a double-channel loop iteration network was designed, where the edge gradient was used in the edge channel to sample the main edge structure and bilateral filtering was used in the non-edge channel to extract the detailed texture feature information. Finally, the feature information extracted from two channels was cyclically iterated to obtain a clear image using the deblurring model with maximum a posteriori probability. The experimental results showed that the image evaluation indexes obtained by the proposed deblurring model were superior to those of other algorithms, and the edge structure and texture details of the image were effectively recovered with better performance.

Key words: double-channel loop iteration; bilateral filtering; image edge gradient; maximum a posteriori probability; image deblurring

0 Introduction

In the process of image acquisition, there may be some interference, making the image blurred. Therefore, without changing hardware equipment and knowing the cause of blur image, it is necessary to use the blind image deblurring algorithm to improve the image quality.

At present, the research on blind image deblurring is mainly divided into image deblurring based on prior knowledge and image deblurring based on deep learning.

The image deblurring method based on prior knowledge uses prior knowledge to constrain image solving, and then uses iteration algorithms to gradually restore clear images. This method is roughly divided into three categories. The first is the image deblurring method based on variable decibel Bayesian (VB) [1], which usually uses prior knowledge to maximize the marginal distribution of the statistical features of the blurred kernel for estimation. The second is the image deblurring method based on maximum a posteriori probability (MAP), which was first proposed by Levin et al.[2] and then developed by Krishnan et al.[3] by using regularization constraints to restore clear images. Additionally, Xu et al.[4] developed an unnatural sparse expression that reduces the runing time, and Cao et al.[5] proposed a blind image deblurring method combining multiple priors such as dark channel priors, gradient priors, and intensity priors. The third is image deblurring method of salience edge selection, which obtains blurred kernel by estimating salience edge. Jia et al.[6] first extracted important edge features of images by using image matting technology. Ding et al.[7] proposed an edge-oriented diffusion equation to restore text images, but it was still difficult to solve the problem of restored images. Yang et al.[8] proposed a joint image restoration and edge detection algorithm in cooperative game formulation, with a new weighted sparse regular term as noise weight to detect image edges. Cui et al.[9] proposed an edge-driven wavelet frame model for image restoration, approximating the image as a piecesmart smoothing function, and restoring the image by applying regularization of different intensity to the smooth and edge regions of the image.

Most image deblurring methods based on deep learning directly utilize the nonlinear characteristics of deep learning algorithms to learn the mapping from blurred images to clear images, thus deblurring without

considering the prior knowledge of image blurring. For example, the combination of generative adversarial network and feature pyramid network could restore the detailed texture and small object features in the image, but with high time complexity[10]. The moving image deblurring algorithm based on spatially variable neural network[11] restores clear images via the features extracted by convolutional neural network. In addition, on the basis of generative adversarial networks, a sparse regularization method is introduced into the embedded layer of the network to obtain a discriminant prior algorithm of the anti-channel[12]. The embedded network of light-dark channel priors[13] inserts channel priors into neural networks to effectively deblur dynamic scenes. However, since the causes of image blurring are complex and varied, as well as the limitations of blur image training datasets, most image deblurring methods based on deep learning could only train specific images, resulting in poor adaptability to all images and a huge amount of training time[14].

In this study, a double-channel cyclic image deblurring algorithm based on edge features is proposed. The algorithm deblurs and restores the image when the cause of image blur is unknown, so as to improve the image sharpness. According to the statistical characteristics of image edge gradient on clear and blur images, the algorithm introduces edge selection and constructs a double-channel cyclic iterative network. The edge gradient operator is taken as a prior term to restore the main edge structure on the edge channel, and the texture details are restored by bilateral filtering on the non-edge channel, thus ensuring the clarity of the image and greatly reducing the time complexity of the algorithm.

1 Basic theory

1.1 Degradation model on image blurring

In the field of image processing and computer vision, image blind deblurring is regarded as a highly ill-posed problem where a clear image and a blurred kernel are solved by a known blurred image. With the homogeneous and spatially invariant assumption, the blurring process is established to be the mathematical model as

$$\boldsymbol{B}=\boldsymbol{I}\otimes\boldsymbol{k}+\boldsymbol{n}, \tag{1}$$

where $\boldsymbol{B}$ stands for a blurred image, $\boldsymbol{I}$ is a potentially clear image, $\boldsymbol{k}$ denotes a blurred kernel, $\boldsymbol{n}$ represents unavoidable noise, and $\otimes$ denotes a convolution operator. In Eq. (1), $\boldsymbol{B}$ is known and $\boldsymbol{I}$ and $\boldsymbol{k}$ are unknown. Since different $\boldsymbol{I}$ and $\boldsymbol{k}$ produce the same $\boldsymbol{B}$, the solution process of Eq. (1) becomes extremely difficult. To solve Eq. (1), a prior knowledge of the image needs to be introduced into Eq. (1) to constrain the clear image.

1.2 Image deblurring model based on MAP

Based on MAP, the image blind deblurring problem is to obtain the maximum statistical feature of the potentially clear image $\boldsymbol{I}$ and the blur kernel $\boldsymbol{k}$ in term of the known blurred image $\boldsymbol{B}$. Namely, given the known blurred image $\boldsymbol{B}$, the joint posterior probability $p(\boldsymbol{k},\boldsymbol{I}|\boldsymbol{B})$ of $\boldsymbol{I}$ and $\boldsymbol{k}$ is estimated by

$$(\boldsymbol{k},\boldsymbol{I})=\arg\max_{\boldsymbol{k},\boldsymbol{I}} p(\boldsymbol{k},\boldsymbol{I}|\boldsymbol{B})=$$
$$\arg\max_{\boldsymbol{k}} p(\boldsymbol{B}|\boldsymbol{k},\boldsymbol{I})\,p(\boldsymbol{I})\,p(\boldsymbol{k}). \tag{2}$$

The log of both ends of Eq. (2) is taken as

$$(\boldsymbol{k},\boldsymbol{I})=\arg\max_{\boldsymbol{k},\boldsymbol{I}} \log p(\boldsymbol{k},\boldsymbol{I}|\boldsymbol{B})=$$
$$\arg\max_{\boldsymbol{k}} \left\{\log p(\boldsymbol{B}|\boldsymbol{k},\boldsymbol{I})+\log p(\boldsymbol{I})+\log p(\boldsymbol{k})\right\}. \tag{3}$$

The estimation of the maximum value on $p(\boldsymbol{k},\boldsymbol{I}|\boldsymbol{B})$ is equivalent to the minimum residual of $\|\boldsymbol{I}\otimes\boldsymbol{k}-\boldsymbol{B}\|$ as

$$(\boldsymbol{k},\boldsymbol{I})=\arg\min_{\boldsymbol{k},\boldsymbol{I}} \|\boldsymbol{I}\otimes\boldsymbol{k}-\boldsymbol{B}\|+\alpha\phi(\boldsymbol{I})+\beta\varphi(\boldsymbol{k}), \tag{4}$$

where $\|\boldsymbol{I}\otimes\boldsymbol{k}-\boldsymbol{B}\|$ is the data fidelity term, which represents the residual of the blurred image $\boldsymbol{B}$ and the convolution operation of $\boldsymbol{I}$ and $\boldsymbol{k}$; $\phi(\boldsymbol{I})$ and $\varphi(\boldsymbol{k})$ are the constraint terms about $\boldsymbol{I}$ and $\boldsymbol{k}$, respectively; and α and β are the corresponding weight parameters.

The image gradient $\nabla\boldsymbol{I}$ is usually used to constrain the potential image. Based on Eq. (4), most of the image deblurring models based on MAP are expressed as

$$\arg\min_{\boldsymbol{I},\boldsymbol{k}} \|\boldsymbol{I}\otimes\boldsymbol{k}-\boldsymbol{B}\|_2^2+\alpha\|\nabla\boldsymbol{I}\|_0+\beta\|\boldsymbol{k}\|_2^2, \tag{5}$$

where l_2 norm constraints are used in the first term and the third term; the data fidelity term $\|I\otimes k-B\|_2^2$ is the similarity between the observed blurred image $\boldsymbol{B}$ and the convolution results of $\boldsymbol{I}$ and $\boldsymbol{k}$; $\|\nabla I\|_0$ uses l_0 norm constraint to ensure that the skeleton image is not affected by removing the tiny deleterious structures with sparseness; and $\|\boldsymbol{k}\|_2^2$ is used to remove the kernel noise to ensure that the kernel is smooth.

The idea of image deblurring methods based on MAP is that the alternately iterative minimum of the objective function on $\boldsymbol{k}$ and $\boldsymbol{I}$ are calculated until a local solution is obtained by the convergence.

1.3 Multi-scale coarse-to-fine strategy of image pyramids

In the multi-scale model, the gray images obtained from different resolutions of the same image are sampled to obtain different feature information at different resolution scales for the image deblurring. More detailed information is obtained at a higher resolution scale sampling and the overall trend of image changes is grasped at a lower resolution scale sampling.

Image pyramid is one of the important image multi-scale models. Fergus et al.[1] applied a "coarse-to-fine" strategy to the image pyramid.

Firstly, the gray image with the most rough resolution is that with the minimum resolution, and the main structure and rough initial blur kernel of the image are extracted by down-sampling. Then, the gray image with higher resolution is further up-sampled by a finer scale to extract more texture detail feature information. Finally, the clear image and final blur kernel are obtained step by step.

However, there exist many problems in multi-scale networks, such as large computation, long time-consuming, difficulty of the parameter settings at each scale, and a large number of experiments to select the appropriate parameters. Therefore, a double-channel cyclic iteration network is designed.

2 Double-channel cyclic image deblurring algorithm

Prior knowledge is the key to solve the ill-posed problem of image deblurring, and the gradient of an image is the easily exacted information with high information entropy. In the gradient image, the part with higher gradient is closer to the edge of visual observation by the human eye. Aiming at the blurring edges in the blurred image, the gradient prior is used to constrain image restoration[14]. The maximum gradient of the image is reduced by obfuscation. Based on this, the maximum gradient of image is introduced to be a differentiation threshold between image edge channels and non-edge channels. The edge gradient is used to extract the main edge structure on the edge channel, and the bilateral filtering is utilized to extract the texture feature information on non-edge channels. Finally, a double channel cyclic iteration network based on MAP deblurring model is proposed for image deblurring. The flow chart of the proposed algorithm is shown in Fig.1.

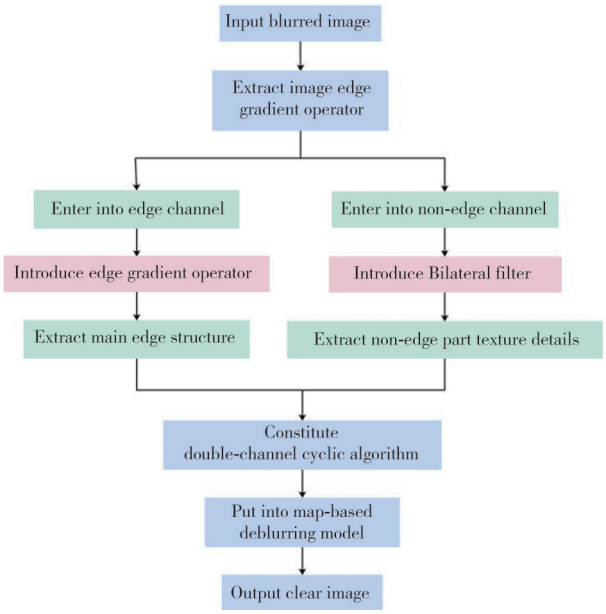

Fig. 1 Flow chart of proposed algorithm

2.1 Edge gradient of image

The deblurring of the image is to improve the clarity of the image. For most of the blurred images, blurring edges mainly result in blurred images. Therefore, the deblurring algorithm based on the recovery of image edges is proposed. According to the experiment in Ref.[15], the gradient value at the edge of the image is higher in the gradient image. According to the experiment in Ref.[16], the maximum gradient value of a clear image becomes lower after the image is blurred. Therefore, the maximum gradient of the image is taken to be the edge gradient of image in this study.

The maximum gradient of the image is defined as

$$M(I(x))=\max_{y\in N(x)}\left(\max_{c\in\{r,g,b\}}\left|\nabla I^{c}(y)\right|\right), \tag{6}$$

where x and y are the pixel positions; $N(x)$ denotes a patch block centered at x; r, g, b are red, green, blue color channels, respectively; and $\nabla I^{c}(y)$ denotes the 2D gradient operator of the image. If $\boldsymbol{I}$ is a gray image, $\max_{c\in\{r,g,b\}}\left|\nabla I^{c}(y)\right|=\left|\nabla I(y)\right|$. Based on Eq. (6), the maximum gradient $M(\cdot)$ of the image is regarded to be an image edge gradient operator for distinguishing edge channels from non-edge channels.

In the following, we show that the maximum gradient of the image is reduced by obfuscation as

$$M(B(x))\leqslant M(I(x)). \tag{7}$$

Let x be the pixel position of the blurred image B. Then,

$$M(B(x))=\max_{y\in N(x)}|\nabla B(y)|=\max_{y\in N(x)}|\nabla(I(y)\otimes k)|=\max_{y\in N(x)}|\nabla I(y)\otimes k|\leqslant\max_{y\in N(x)}|\nabla I(y)|\cdot|k|=\max_{y\in N(x)}|\nabla I(y)|=M(I(x)). \tag{8}$$

In Eq(8), the derivation from the third step to the fourth step can be proved by use of Young's convolution inequality[17], and the derivation from the fourth step to the fifth step is that the obfuscation is taken to be the convolution operation between the clear image and the blur kernel. Then, $|\boldsymbol{k}|=\sum_{z\in\Omega_k}k(z)=1$, where z is the input of the convolution operation, and Ω_k denotes the definition domain of the blurred kernel.

2.2 Edge channel feature information extracted by image edge gradients

Based on the definition of $M(I)$ in Eq. (6), the max operator and $|\cdot|$ operator are mapping matrices. $|\cdot|$ is the vectorization of image gradient $\nabla\boldsymbol{I}$ to matrix $\boldsymbol{A}$. Every element of $\boldsymbol{A}$ is taken to be -1 or 1, related to the extremum property of $\nabla\boldsymbol{I}$. The gradient operator is $\nabla=(\nabla h,\nabla v)^{\mathrm{T}}$. Therefore, $\boldsymbol{A}=(\boldsymbol{A}_h,\boldsymbol{A}_v)$, where

$$A_h(x,y)=\begin{cases}1, & \nabla I_h(x,y)\geqslant 0,\\ -1, & \nabla I_h(x,y)<0.\end{cases} \tag{9}$$

$$A_v(x,y)=\begin{cases}1, & \nabla I_v(x,y)\geqslant 0,\\ -1, & \nabla I_v(x,y)<0.\end{cases} \tag{10}$$

Then, $|\nabla\boldsymbol{I}|=\boldsymbol{A}\cdot\nabla\boldsymbol{I}$, where $\cdot$ denotes element-wise multiplication of two matrices.

The max operator is replaced by a sparse matrix $\boldsymbol{G}$ as

$$G(x,z)=\begin{cases}1, & z=\arg\max_{y\in N(x)}|\nabla I|(y),\\ 0, & \text{otherwise.}\end{cases} \tag{11}$$

Let $\boldsymbol{H}=\boldsymbol{G}\cdot\boldsymbol{A}\cdot\nabla$, and then

$$M(I)=\boldsymbol{H}\cdot\boldsymbol{I}. \tag{12}$$

Therefore, the obtained $M(I)$ is the feature information extracted from the image edge channels.

2.3 Non-edge channel feature information extracted by bilateral filtering

Bilateral filtering[15] is that the pixel value similarity weights are introduced into the Gaussian filtering to remove the noise and preserve the clarity of the image. In an image, the pixel variation is low in some flat areas where Gaussian filtering can be used directly to reduce the noise. However, in most of the image edges, the pixel values tend to change drastically and the pixel values on both sides of the edges are vastly different, therefore, the pixel similarity weights are introduced to carry out the constraints on the pixel values. Suppose that a region S that contains the image edges is found, which is divided into two pieces A, B by the image edge, and then a center point is found in this region. During the noise reduction, more weights are given to the region similar to the center point. Namely, if the center point is close to the junction of A and B and is within A, the given weights of the pixels at A are higher than those at B when the pixel value of the center point is calculated.

The weights of distance and similarity are considered in the bilateral filtering, we have

$$\bar{I}(x)=\frac{1}{w_x}\sum_{y\in S}G_d\left(\|x-y\|\right)G_c\left(\left|I(x)-I(y)\right|\right)I(y), \tag{13}$$

where $w_x=\sum_{y\in S}G_d\left(\|x-y\|\right)G_c\left(\left|I(x)-I(y)\right|\right)$; x and y are the positions of the target pixel and any pixel, respectively; $I(x)$ and $I(y)$ are the pixel values at x and y, respectively; $\bar{I}(x)$ is the pixel value at x by the bilateral filtering; and $G_d\left(\|x-y\|\right)$ and $G_c\left(\|x-y\|\right)$ are defined as

$$G_d\left(\|x-y\|\right)=\exp\left(-\frac{\|x-y\|}{2\delta_d^2}\right), \tag{14}$$

$$G_c\left(\left|I(x)-I(y)\right|\right)=\exp\left(-\frac{\left|I(x)-I(y)\right|}{2\delta_c^2}\right), \tag{15}$$

where $\|x-y\|$ denotes the Euclidean distance between the pixel points x and y; $\left|I(x)-I(y)\right|$ represents the absolute value of the difference of pixel values between pixel points x and y; and δ_d^2 and δ_c^2 represent the two standard deviations.

In this study, the bilateral filtering is utilized to extract the feature information from the non-edge part of the image.

2.4 Image fusion by a double-channel loop algorithm

The image is divided into edge channel and non-edge channel by the edge gradient operator. The edge feature information is extracted by the edge gradient at the edge channel and the texture details are extracted by the bilateral filtering at the non-edge channel. Then, the convolutional results of the edge feature information, the estimated blur kernel and the minimum loss function of the blurred image are used to determine the parameter weights shared at the non-edge channel. Thus, the double-channel loop algorithm is established.

In this study, l_1 norm is utilized to constrain $M(I)$, $\|M(I)\|_1$ is applied to the image deblurring model based on MAP, and the corresponding image deblurring model is expressed as

$$\min_{I,k} \|I \otimes k - B\|_2^2 + \alpha\|M(I)\|_1 + \beta\|\nabla I\|_0 + \gamma\|k\|_2^2, \quad (16)$$

where α, β and γ are the coefficients of the regularization terms, the first term is a data fidelity term to ensure the similarity between the observed blurred image B and the obtained image $I \otimes k$ by the convolution of the clear image I and the blur kernel k, the second term is our newly added regularization term, the third term is used to ensure the texture details, and the last term can constrain the kernel noise to ensure that the blur kernel is smooth.

Since the direct solution of Eq. (16) has the large and complex computation, the image deblurring problem from Eq. (16) is decomposed into two sub-problems Eqs. (17) and (18) by the coordinate descent method. Eqs. (17) and (18) are solved alternatively to estimate the clear intermediate potential image and the blur kernel, respectively.

$$\begin{cases} \min\limits_{I} \| I \otimes k - B \|_2^2 + \alpha \| M(I) \|_1 + \beta \| \nabla I \|_0, & (17) \\ \min\limits_{k} \| I \otimes k - B \|_2^2 + \gamma \| k \|_2^2. & (18) \end{cases}$$

The double-channel loop iteration algorithm is designed to estimate the clear potential image I and the blur kernel k, where the blurred image B is regarded as the input image I_0. The concrete steps are as follows:

Step 1) The input image I_0 is substituted into Eq. (18) to extract the main edge information and the blur kernel k_1 is obtained by half quadratic splitting method.

Step 2) The potential edge image I_1 is obtained from Eq. (17) based on the blur kernel k_1.

Step 3) The detailed texture information image I_2 extracted is obtained from the potential image I_1 by the bilateral filtering.

Step 4) The blur kernel k_2 is obtained from Eq. (18) based on I_2.

Step 5) If the termination conditions are met, the final clear image $I = I_2$ and the blur kerne $k = k_2$ are obtained. Otherwise, let $I_1 = I_2$ and $k_1 = k_2$, then turn to Step 2.

The flow chart of the double-channel loop iteration process by n times iterations is shown in Fig.2.

The half quadratic splitting method[19] is used to optimize Eq. (17) by introducing two new variables u and v, where u replaces $M(I)$ and v replaces ∇I. Eq. (17) can be rewritten as

$$\min_{I,u,v} \left(\|I \otimes k - B\|_2^2 + \alpha'\|u\|_1 + \beta'\|v\|_0 + \alpha\|M(I) - u\|_2^2 + \beta\|\nabla I - v\|_2^2 \right), \quad (19)$$

where α' and β' are the penalty parameters. Substituting Eq. (12) into Eq. (19), we have

$$\min_{I,u,v} \left(\|I \otimes k - B\|_2^2 + \alpha'\|u\|_1 + \beta'\|v\|_0 \alpha\|H \bullet I - u\|_2^2 + \beta\|\nabla I - v\|_2^2 \right). \quad (20)$$

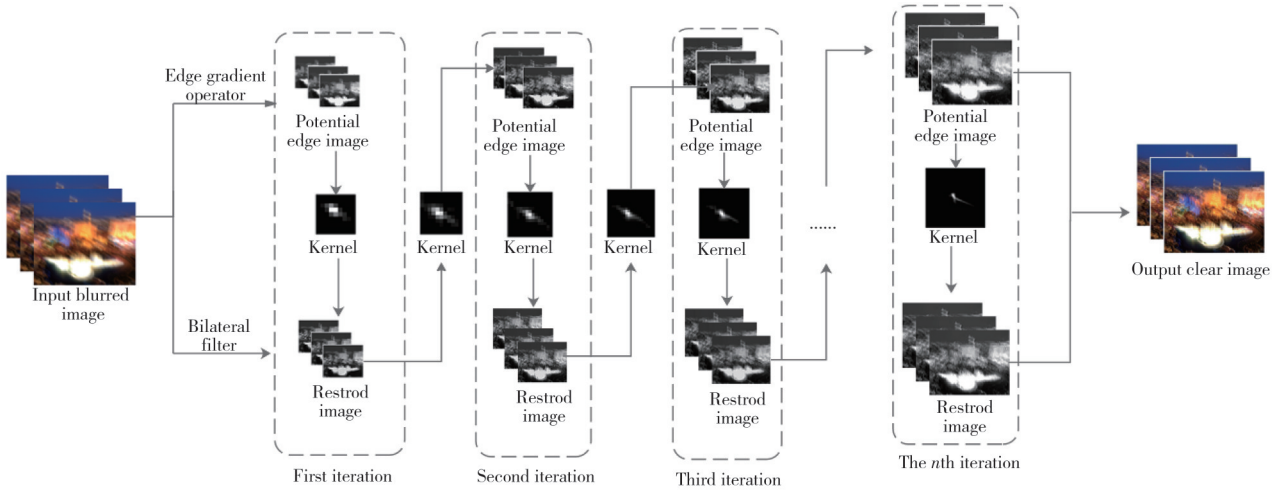

Fig. 2 Flow chart of double-channel loop iteration process

Now, Eq. (20) will be solved by alternating I, u, v optimization.

Firstly, Eq. (21) is obtained by fixing I as

$$\begin{cases} \min\limits_{u} \alpha'\|u\|_1 + \alpha\|H \bullet I - u\|_2^2, \\ \min\limits_{v} \beta'\|v\|_0 + \beta\|\nabla I - v\|_2^2. \end{cases} \quad (21)$$

The solutions of Eq. (21) are

$$u = \operatorname{sgn}(H \bullet I) \bullet \max\left(|H \bullet I| - \frac{\alpha'}{2\alpha}, 0 \right), \quad (22)$$

$$v = \begin{cases} \nabla I, & |\nabla I|^2 \geqslant \dfrac{\beta'}{\beta}, \\ 0, & \text{otherwise.} \end{cases} \quad (23)$$

Substituting Eqs. (22) and (23) into Eq. (20), we

have

$$\min_{I} \|\boldsymbol{I} \otimes \boldsymbol{k} - \boldsymbol{B}\|_2^2 + \alpha \|\boldsymbol{H} \cdot \boldsymbol{I} - \boldsymbol{u}\|_2^2 + \beta \|\nabla \boldsymbol{I} - \boldsymbol{v}\|_2^2. \quad (24)$$

Eq. (24) is solved by the fast Fourier transform (FFT), and the potential edge image $\boldsymbol{I}_1$ is obtained as

$$\boldsymbol{I}_1 = F^{-1}\left(\frac{F(\boldsymbol{k})F(\boldsymbol{B}) + \alpha F(\boldsymbol{H})F(\boldsymbol{u}) + \beta F(\boldsymbol{v}) - \beta F(\nabla \boldsymbol{I})}{\overline{F(\boldsymbol{k})}F(\boldsymbol{k}) + \alpha F(\boldsymbol{H}^{\mathrm{T}}\boldsymbol{H})}\right). \quad (25)$$

The detailed texture information of image $\boldsymbol{I}_2$ extracted from the potential image $\boldsymbol{I}_1$ by the bilateral filtering is substituted into Eq. (13), and finally clear image is obtained $\boldsymbol{I}$.

To speed up the convergence, the kernel estimation method[19] is employed and Eq. (18) is redefined as

$$\min_{k} \|\nabla \boldsymbol{I} \otimes \boldsymbol{k} - \nabla \boldsymbol{B}\|_2^2 + \gamma \|\boldsymbol{k}\|_2^2. \quad (26)$$

The optimal solution of the blur kernel $\boldsymbol{k}$ is obtained directly by FFT.

Thus, the clear image $\boldsymbol{I}$ and the blur kernel $\boldsymbol{k}$ are alternately got by a multi-scale coarse-to-fine image pyramid strategy.

3 Experimental results and analysis

In the experiments, the parameters in Eq. (17) and Eq. (18) were set to α=0.004, β=0.000 1, and γ=1. The size of the image block was 65 during the computation of edge channel via Eq. (16). The experiments were all performed in Matlab R2019a. The computer was Inter(R) Core(TM) i7-10700 CPU @ 2.90 GHz, 8.00 GB of RAM. Three mainstream benchmark datasets were provided by Levin et al.[20], Köhler et al.[21], and GoPro dataset[13].

To verify the effectiveness of the proposed algorithm, the dark channel prior algorithm proposed by Pan et al.[22], the l_1/l_2 regularized sparse prior algorithm proposed by Krishnan et al.[3], and the low-rank sparse prior algorithm proposed by Liu et al.[19], the local minimum intensity prior algorithm by Wen et al.[22], a variety of prior combination algorithm by Cao et al.[5], and the edge retention regular term algorithm by Zhang et al.[23] were selected for comparison. Figs. 3 and 4 are the results of restoring the blurred image from the real world and the blurred images from the synthetic world, respectively.

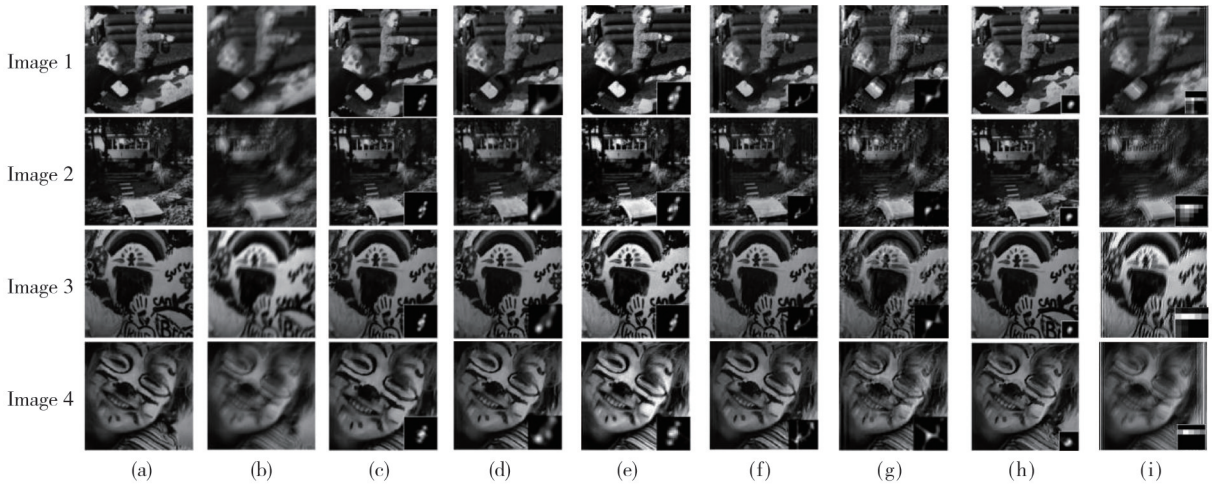

Fig. 3 Comparison of image restoration effects in synthetic world datasets. (a) Clear image; (b) Blurred image; (c) Ours; (d) Pan et al.[21]; (e) Liu et al.[19]; (f) Wen et al.[22]; (g) Krishnan et al.[3]; (h) Cao et al.[5]; (i) Zhang et al.[23]

3.1 Qualitative evaluation of image deblurring

Fig. 3 shows the results of some restored images in the synthetic world datasets. It can be seen that the restored images obtained by our method have more obvious advantages, such as texture details, image main edge structure. Fig. 4 shows the results of some restored images in the real world datasets. It can be seen that better restoration results are from our method, such as texture details and clearness, which means that our algorithm is superior to other algorithms. For the natural landscape image 5, the texture details obtained by our algorithm are the clearest. For the license plate image 6, the license plate number can be observed clearly by our algorithm, but there exist some ghosting by other algorithms. For the face images 7 and 8, the details of the faces obtained by our method are more clearer than that obtained by other compared algorithms, such as details of the eyes. For the text image 9, although the text from the restored image by our algorithm can be seen more clearly, there exists ringing, which means that our algorithm needs to be improved further.

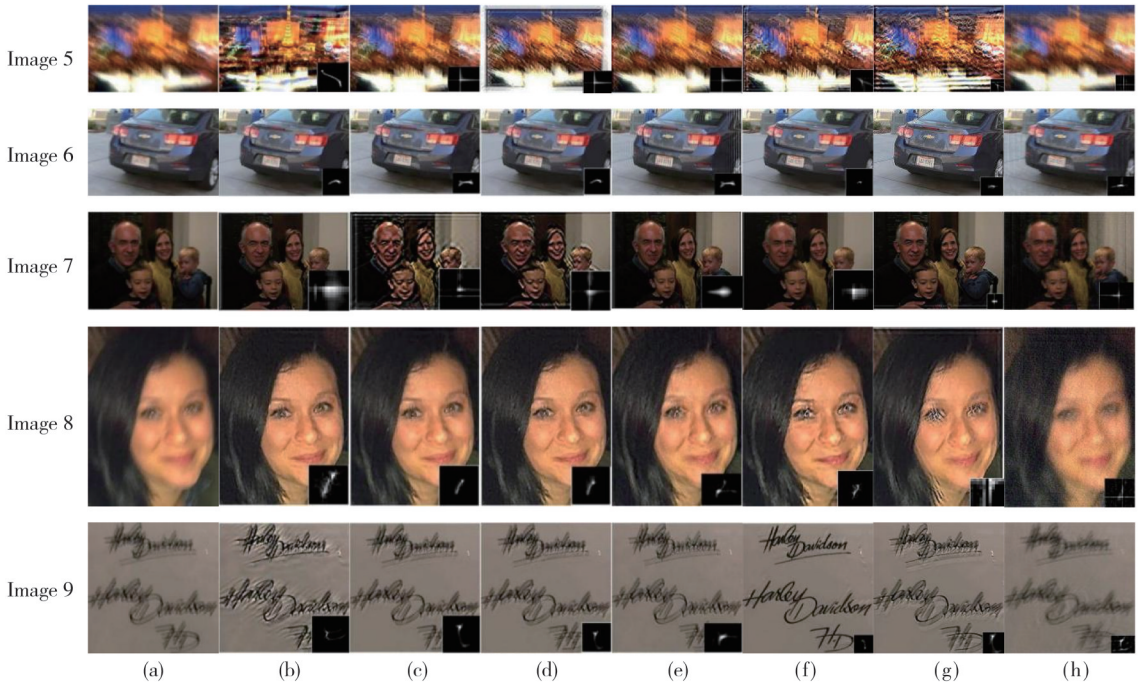

Fig. 4 Comparison of image restoration effects in real world datasets. (a) Blurred image; (b) Ours; (c) Pan et al. [21]; (d) Wen et al. [22]; (e) Krishnan et al. [3]; (f) Cao et al. [5]; (g) Liu et al. [19]; (h) Zhang et al. [23]

3.2 Quantitative evaluation of image deblurring

After the qualitative evaluation and comparison of the deblurring effects of different methods on blur images in Section 3.1, four evaluation indexes, peak signal-to-noise ratio (PSNR), structural similarity (SSIM), graph average gradient (AG) and information entropy (En), are used to evaluate the deblurring effects of different methods. SSIM is a fully referenced image quality evaluation criterion, which is measured from brightness, contrast and structure. The larger the SSIM, the more the restored image similar to the clear image, and the better the restored effect. PSNR is the error between corresponding pixel points, which is used for the image quality evaluation based on error-sensitivity. The larger the PSNR, the smaller the errors between the restored image and the clear image, and the better the restored effect. AG is used to measure the clarity of the restored image. the larger the AG, the better the clarity of the restored image, and the better the restored effect. En reflects the information amount in the image. The larger En, the more information contained in the restored image.

SSIM is defined as

$$\sigma_{\mathrm{SSIM}}(x,y)=l(x,y)c(x,y)s(x,y), \tag{27}$$

where

$$l(x,y)=\frac{2\mu_x\mu_y+C_1}{\mu_x^2+\mu_y^2+C_1},$$

$$c(x,y)=\frac{2\sigma_x\sigma_y+C_2}{\sigma_x^2+\sigma_y^2+C_2},$$

$$s(x,y)=\frac{\sigma_{xy}+C_3}{\sigma_x\sigma_y+C_3},$$

μ_x, μ_y and σ_x, σ_y denote the means and variances of the images x and y, respectively, and C_1, C_2 and C_3 are the constants.

PSNR is defined as

$$\sigma_{\mathrm{PSNR}}=10\lg\frac{\sigma_{\mathrm{MAX}_I^2}}{\sigma_{\mathrm{MSE}}}, \tag{28}$$

$$\sigma_{\mathrm{MSE}}=\frac{1}{M\times N}\sum_{i=1}^{M}\sum_{j=1}^{N}\left[I(i,j)-\hat{I}(i,j)\right]^2, \tag{29}$$

where I and $\hat{I}$ denote the original image and the restored image, respectively, $M\times N$ is the size of the image, (i,j) is the coordinates of the pixel, and $\sigma_{\mathrm{MAX}_I^2}$ is the maximum pixel value of image I.

AG is defined as

$$\sigma_{\mathrm{AG}}=\frac{1}{(M-1)(N-1)}\times\sum_{i=1}^{M-1}\sum_{i=1}^{N-1}\sqrt{\frac{(I(i+1,j)-I(i,j))^2+(I(i,j+1)-I(i,j))^2}{2}}, \tag{30}$$

where I is the deblurred image, $M\times N$ is the size of the image, and (i,j) is the coordinates of the pixel.

En is defined as

$$\sigma_{\mathrm{En}}=-\sum_{i=0}^{255}p_i\lg p_i, \tag{31}$$

where p_i is the proportion of the number of the pixels with the gray value i in the deblurred image.

Tables 1 and 2 are the compared results on PSNR, SSIM, AG, and En by our algorithm and the other algorithms on the images in Figs.3 and 4.

Table 1 Comparison of evaluation indexes obtained by different algorithms in Fig. 3

Image No.	Method	PSNR	SSIM	AG	En
Image 1	Ours	**25.869 5**	**0.851 6**	**11.927 6**	**23.816 1**
	Pan et al.[21]	23.009 1	0.724 3	6.170 1	3.199 3
	Krishnan et al.[3]	18.965 8	0.355 2	7.364 0	2.644 9
	Wen et al.[22]	23.143 3	0.788 9	8.938 6	2.168 5
	Liu et al.[19]	23.028	0.786 4	11.769 1	2.124 1
	Cao et al.[5]	12.410 4	0.284 0	8.024 4	12.410 4
	Zhang et al.[23]	19.114 7	0.820 5	4.810 0	6.932 3
Image 2	Ours	**25.013 7**	0.804 6	**15.520 3**	**36.420 1**
	Pan et al.[21]	23.806 5	0.679 7	7.709 8	1.898 5
	Krishnan et al.[3]	18.965 8	0.374 2	8.920 4	2.248 7
	Wen et al.[22]	23.660 2	0.782 9	9.241 7	4.764 5
	Liu et al.[19]	21.377 8	0.745 4	10.520 3	2.178 7
	Cao et al.[5]	13.497 6	0.286 6	7.963 1	1.923 6
	Zhang et al.[23]	24.591 5	**0.806 3**	4.733 3	11.483 3
Image 3	Ours	**26.020 8**	**0.857 4**	**13.497 6**	**4.270 7**
	Pan et al.[21]	25.823 3	0.817 5	8.862 9	2.702 9
	Krishnan et al.[3]	19.515 7	0.465 6	8.765 9	2.084 2
	Wen et al.[22]	23.696 5	0.822 5	9.937 8	2.457 3
	Liu et al.[19]	17.064 3	0.706 1	10.204 8	2.249 4
	Cao et al.[5]	13.046 8	0.270 7	8.657 2	2.708 9
	Zhang et al.[23]	16.265 2	0.554 1	10.745 9	2.083 8
Image 4	Ours	**29.635 4**	**0.901 2**	**7.358 0**	**2.700 3**
	Pan et al.[21]	26.658 8	0.852 6	7.179 8	2.602 2
	Krishnan et al.[3]	19.735 5	0.474 7	6.258 7	2.460 8
	Wen et al.[22]	24.114	0.852 7	6.205 6	2.148 1
	Liu et al.[19]	17.981 4	0.745 9	7.119 1	2.591 6
	Cao et al.[5]	14.561 5	0.296 1	7.266 6	2.103 5
	Zhang et al.[23]	16.226 1	0.710 0	4.899 2	1.446 7

It can be seen from the data in Table 1, the indexes of PSNR, SSIM, AG and En obtained by our method are all higher than those obtained by the other algorithms for the synthestic world images, indicating that the recovered image obtained by our algorithm has more complete structure information, less distortion, higher image quality, and less loss of brightness and contrast, thereby having better deblurring effect.

It can be seen from Table 2 that for real-world images, PSNR, SSIM, AG and En of evaluation indicators obtained by the proposed method are mostly higher than those obtained by the comparison algorithm, indicating that the image has higher clarity and contains more information, and the proposed method has better performance in deblurring.

Table2 Comparison of evaluation indexes obtained by different algorithms in Fig. 4

Image No.	Method	PSNR	SSIM	AG	En
Image 5	Ours	**24.315 2**	**0.656 2**	**11.167 2**	**10.258 9**
	Pan et al.[21]	18.897 7	0.455 1	4.751 4	0.619 3
	Krishnan et al.[3]	16.657 1	0.233 6	5.743 1	1.913 9
	Wen et al.[22]	15.193 2	0.255 1	5.829 4	0.373 8
	Liu et al.[19]	17.210 0	0.373 0	9.996 5	2.499 7
	Cao et al.[5]	18.010 2	0.338 5	8.124 0	6.901 4
	Zhang et al.[23]	23.951 8	0.517 3	8.215 3	5.936 2
Image 6	Ours	**27.677 0**	**0.877 3**	**5.844 7**	6.669 8
	Pan et al.[21]	25.021 7	0.736 5	4.142 0	1.930 5
	Krishnan et al.[3]	22.453 8	0.652 8	4.367 9	2.631 4
	Wen et al.[22]	26.107 7	0.793 1	4.343 6	2.748 0
	Liu et al.[19]	19.353 0	0.539 6	5.622 8	3.300 2
	Cao et al.[5]	24.241 6	0.717 6	4.848 2	**7.432 3**
	Zhang et al.[23]	24.956 5	0.661 5	2.130 3	5.336 4
Image 7	Ours	**24.893 6**	**0.849 5**	**10.477 6**	6.460 8
	Pan et al.[21]	22.596 4	0.792 1	6.897 5	1.845 5
	Krishnan et al.[3]	24.390 2	0.815 5	6.088 9	**9.148 1**
	Wen et al.[22]	22.364 3	0.638 5	6.258 7	3.538 8
	Liu et al.[19]	21.148 7	0.820 5	5.763 4	5.607 8
	Cao et al.[5]	17.493 5	0.473 7	4.726 9	6.284 5
	Zhang et al.[23]	23.956 5	0.650 7	10.361 5	5.440 1
Image 8	Ours	**30.684 1**	**0.806 8**	**6.710 0**	**10.972 6**
	Pan et al.[21]	28.127 6	0.692 0	5.271 1	1.930 9
	Krishnan et al.[3]	28.999 3	0.698 1	6.205 6	2.073 3
	Wen et al.[22]	26.034 0	0.719 5	6.255 8	6.640 0
	Liu et al.[19]	21.178 2	0.678 0	6.023 8	3.571 5
	Cao et al.[5]	26.555 1	0.722 9	5.138 2	8.937 2
	Zhang et al.[23]	25.029 4	0.353 3	5.098 3	9.186 9
Image 9	Ours	**27.431 3**	**0.862 6**	**6.590 3**	**18.269 3**
	Pan et al.[21]	24.647 2	0.651 1	1.677 8	1.462 1
	Krishnan et al.[3]	21.644 8	0.674 8	4.048 7	4.426 1
	Wen et al.[22]	20.111 7	0.528 1	3.589 3	4.817 8
	Liu et al.[19]	23.587 9	0.626 9	4.301 0	7.938 1
	Cao et al.[5]	18.220 0	0.472 9	4.056 5	3.932 8
	Zhang et al.[23]	26.824 8	0.828 7	2.527 5	3.994 7

To verify the operation rate of the proposed algorithm, taking the average running time on the blurred images with different sizes on Fig.4 for comparison. Table 3 shows the time complexity from image 1 to image 9. It is found that the running time of the proposed method is less than those of other algorithms, which indicates that the time complexity of the proposed algorithm is small, which is more beneficial to batch deblurring multiple images.

Table 3 Comparison of running time of different algorithms

Resolution/ pixels per inch	Running time/s						
	Ours	Pan et al.[21]	Krishnan et al.[3]	Wen et al.[22]	Liu et al.[19]	Cao et al.[5]	Zhang et al.[23]
256×256	**126.59**	215.96	512.37	384.09	876.52	789.12	198.13
512×512	**387.97**	608.35	872.41	824.67	1 230.21	1 028.26	572.49
768×768	**551.23**	958.16	1 238.71	1 152.03	1 630.78	1 325.26	701.13
1 024×1 024	**757.84**	1 005.90	1 691.28	1 524.06	2 012.31	1 826.78	813.52

3.3 Validity evaluation of $\|M(I)\|_1$

The regular term $\|M(I)\|_1$ were added to the deblurring model in Section 2.4 previously. The experimental results in Sections 3.1 and 3.2 show that the proposed method has better deblurring effect, but it does not specifically verify the validity of $\|M(I)\|_1$. In this section, we will provide more examples that visually illustrate the difference between the images with and without $\|M(I)\|_1$, as shown in Fig.5.

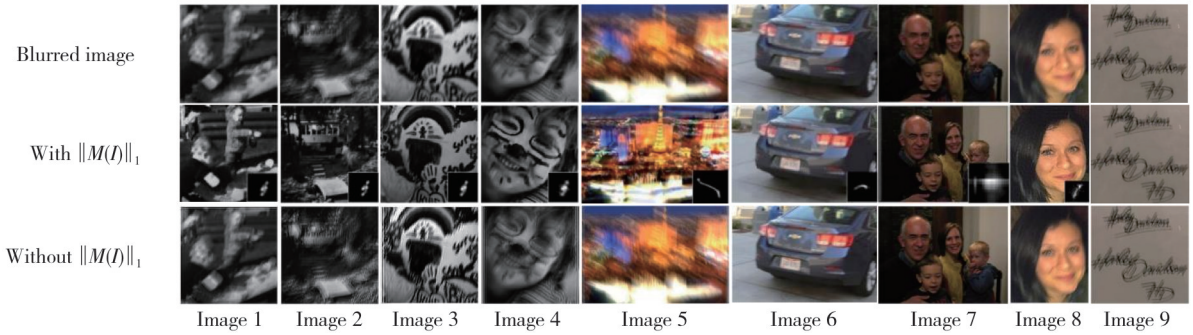

Fig. 5 Comparison of images with $\|M(I)\|_1$ and without $\|M(I)\|_1$

It can be seen that the restored images without $\|M(I)\|_1$ have little difference with the blurred images, and the image restoration effect is poor, while the restored images by deblurring algorithm with $\|M(I)\|_1$ are clearer, and the clarity of texture details has been significantly improved. Therefore, the validity of the regular term $\|M(I)\|_1$ is evaluated.

4 Conclusions

Aiming at the blurring in images caused by various reasons, the double-channel loop deblurring algorithm based on edge features was proposed. A double-channel cyclic iteration algorithm was designed, the edge gradient was taken as the discrimination threshold to distinguish edge channels from the non-edge channels. The main edge structure of the image was obtained at the edge channel and the image details and texture information were obtained at the non-edge channels. Afterwards, the image was substituted into the deblurring model based on MAP to be deblurred. The experimental results show that the proposed algorithm can effectively deal with the blurring images, and improve deblurring effectiveness. This method can be applied to the deblurring in real images universally. However, for the image datasets with the complex scenes, since different objects have different degree of blurriness, there are still some blurry residues in the deblurred image by our method, which will be the direction of future efforts.

Acknowledgement

This work was supported in part by Natural Science Research Foundation of Shanxi Province (Nos. 20210302123019, 20210302124195, 20210302124212, 20210302123189)

Declaration of conflicting interests

The authors have no conflict of interests related to this publication.

References

[1] FERGUS R, SINGH B, HERTZMANN A, et al. Removing camera shake from a single photograph//ACM SIGGRAPH 2006 Papers, July 30, 2006, Boston, Massachusetts, USA. New York: ACM, 2006: 787-794.

[2] LEVIN A, WEISS Y, DURAND F, et al. Efficient marginal likelihood optimization in blind deconvolution// CVPR 2011, June 20-25, 2011, Colorado Springs, CO, USA. New York: IEEE, 2011: 2657-2664.

[3] KRISHNAN D, TAY T, FERGUS R. Blind deconvolution using a normalized sparsity measure//2011 IEEE Conference on Computer Vision and Pattern Recoggnition, June 20-25, 2011, Colorado Springs, CO, USA. New York: IEEE, 2011: 233-240.

[4] XU L, ZHENG S C, JIA J Y. Unnatural L0 sparse representation for natural image deblurring//2013 IEEE Conference on Computer Vision and Pattern Recognition, June 23-28, 2013, Portland, OR, USA. New York: IEEE, 2013: 1107-1114.

[5] CAO S F, HU H P, WANG W K. Blind image deblurring method based on l_1/l_2-norm regularization. Journal of Measurement Science and Instrumentation, 2023, 14(2): 182-188.

[6] JIA J Y. Single image motion deblurring using transparency//2007 IEEE Conference on Computer Vision and Pattern Recognition, June 17-22, 2007, Minneapolis, MN, USA. New York: IEEE, 2007: 1-8.

[7] DING M N. An edge-directed diffusion equation-based image restoration approach for font generation. IEEE Access, 2023, 11: 141435-141444.

[8] YANG C Y, WANG W W, FENG X C. Joint image restoration and edge detection in cooperative game formulation. Signal Processing, 2022, 191: 108363.
[9] CHOI J K, DONG B, ZHANG X Q. An edge driven wavelet frame model for image restoration. Applied and Computational Harmonic Analysis, 2020, 48(3): 993-1029.
[10] LI R Q, CANG Y. A lightweight blind super resulotion network based on generative adversarial network. Applied Science and Technology, 2024, 51(2): 112-119.
[11] ZHANG J W, PAN J S, REN J, et al. Dynamic scene deblurring using spatially variant recurrent neural networks//2018 IEEE/CVF Conference on Computer Vision and Pattern Recognition, June 18-23, 2018, Salt Lake City, UT, USA. New York: IEEE, 2018: 2521-2529.
[12] SHAO W Z, LIU Y Y, YE L Y, et al. DeblurGAN+: Revisiting blind motion deblurring using conditional adversarial networks. Signal Processing, 2020, 168: 107338.
[13] CAI J R, ZUO W M, ZHANG L. Dark and bright channel prior embedded network for dynamic scene deblurring. IEEE Transactions on Image Processing, 2020, 29: 6885-6897.
[14] CAO H J, LI Y F, ZHANG Q A. An improved fundus image repair algorithm Criminisi. Journal of North University of China (Natural Science Edition), 2023, 44(2): 176-181.
[15] SHAN Q, JIA J Y, AGARWALA A. High-quality motion deblurring from a single image. ACM Transactions on Graphics, 2008, 27(3): 1-10.
[16] FERGUS R, SINGH B, HERTZMANN A, et al. Removing camera shake from a single photograph//ACM SIGGRAPH 2006 Papers, July 30, 2006, Boston, Massachusetts. New York: ACM, 2006: 787-794.
[17] ZHANG K, ZUO W M, CHEN Y J, et al. Beyond a Gaussian denoiser: residual learning of deep CNN for image denoising. IEEE Transactions on Image Processing, 2017, 26(7): 3142-3155.
[18] YOUNG W H. On the multiplication of successions of Fourier constants. Proceedings of the Royal Society of London Series A, Containing Papers of a Mathematical and Physical Character, 1912, 87(596): 331-339.
[19] PAN J S, LIU R S, SU Z X, et al. Motion blur kernel estimation *via* salient edges and low rank prior//2014 IEEE International Conference on Multimedia and Expo, July 14-18, 2014, Chengdu, China. New York: IEEE, 2014: 1-6.
[20] LEVIN A, WEISS Y, DURAND F, et al. Efficient marginal likelihood optimization in blind deconvolution//2011 IEEE Conference on Computer Vision and Pattern Recognition, June 20-25, 2011, Colorado Springs, CO, USA. New York: IEEE, 2011: 2657-2664.
[21] PAN J S, SUN D Q, PFISTER H, et al. Blind image deblurring using dark channel prior//2016 IEEE Conference on Computer Vision and Pattern Recognition, June 27-30, 2016, Las Vegas, NV, USA. New York: IEEE, 2016: 1628-1636.
[22] WEN F, YING R D, LIU Y P, et al. A simple local minimal intensity prior and an improved algorithm for blind image deblurring. IEEE Transactions on Circuits and Systems for Video Technology, 2021, 31(8): 2923-2937.
[23] ZHANG Y Z, SHI Y, MA L, et al. Blind natural image deblurring with edge preservation based on L0-regularized gradient prior. Optik, 2021, 225: 1657.

基于边缘特征的双通道循环图像去模糊算法

李佳敏, 胡红萍*, 白艳萍

中北大学 数学学院, 山西 太原 030051

摘　要： 人们拍摄的照片经常由于抖动、失焦、景深变化、拍摄物体运动等问题而变得模糊，针对这一现象，提出了基于边缘特征的双通道循环图像去模糊方法。首先，根据经模糊处理后图像边缘梯度最大值会减小这一规律引入了图像边缘梯度算子，并将其作为阈值将模糊图像来划分为两个通道：边缘通道和非边缘通道。其次，设计了双通道循环迭代网络，在边缘通道上利用边缘梯度对主要边缘结构进行采样，在非边缘通道上利用双边滤波提取细节纹理特征信息。最后，将两个通道提取的特征信息进行循环迭代，利用最大后验概率的去模糊模型得到清晰图像。实验结果表明，所提出的去模糊模型得到的图像评价指标均高于其他算法，有效恢复了图像边缘结构和纹理细节，性能较好。

关键词： 双通道循环迭代；双边滤波；图像边缘梯度；最大后验概率

引用格式： LI Jiamin, HU Hongping, BAI Yanping. Double-channel cyclic image deblurring algorithm based on edge features. Journal of Measurement Science and Instrumentation, 2025, 16(1): 75-84. DOI: 10.62756/jmsi.1674-8042.2025008